Synthesis and Design of Terbium-Activated $CaWO_4$ Nanocrystals for Fluorescence Sensing of Alkaline Phosphatase and Bioimaging Applications

Terefe Tafese Bezuneh[1,5], Xin Li[1], Tongtong Kou[1], Fuchun Nan[1], Zilong Wu[1], Lanbo Shen[2], Xinyuan Xia[3], Bin Li[2,*], Liang Wang[4,*], William W. Yu[1,*]

1. School of Chemistry and Chemical Engineering, Ministry of Education Key Laboratory of Special Functional Aggregated Materials, Shandong Key Laboratory of Advanced Organosilicon Materials and Technologies, Shandong University, Jinan 250100; Shandong Provincial Key Laboratory for Science of Material Creation and Energy Conversion, Science Center for Material Creation and Energy Conversion, Shandong University, Qingdao 266237, China

2. Research Center of Translational Medicine, Central Hospital Affiliated to Shandong First Medical University, Jinan 250013, China

3. College of Chemistry, Chemical Engineering and Materials Science, Shandong Normal University, Jinan 250014, China

4. School of Integrated Circuits, Shandong University, Jinan 250100, China

5. Department of Chemistry, College of Natural Sciences, Arba Minch University, P. O. Box 21, Arba Minch, Ethiopia

* Corresponding authors: qingquan0615@163.com (B. Li), liangwang2023@sdu.edu.cn (L. Wang), wyu6000@gmail.com (W. W. Yu)

Optimization of synthesis parameters

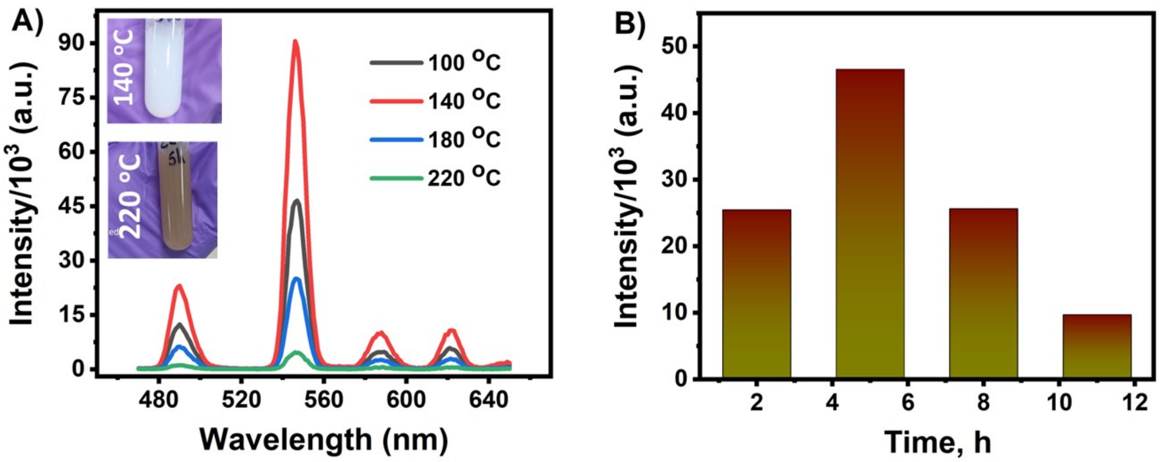

Fig. S1 Optimization of synthesis parameters A) temperature: insets are corresponding aqueous dispersion of PEG-Tb-$CaWO_4$ NCs and B) time.

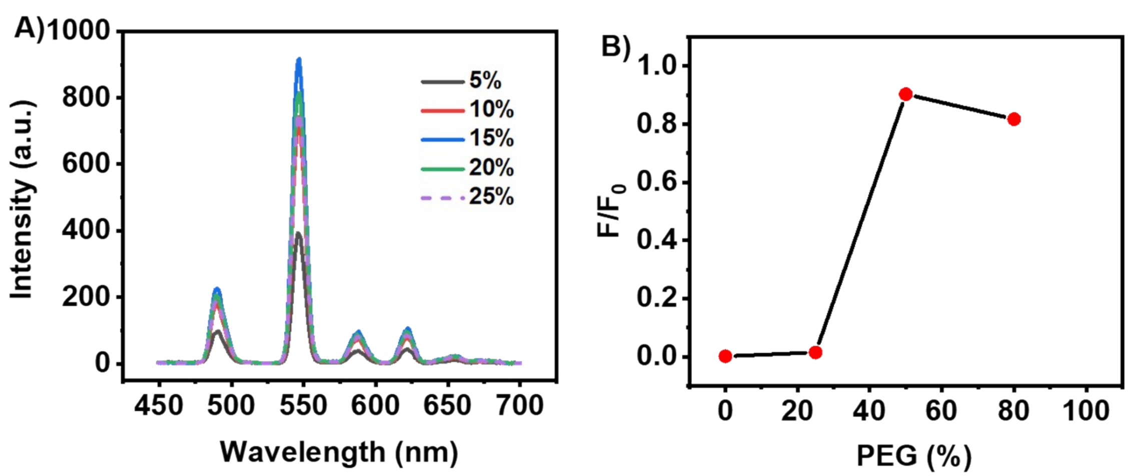

Fig. S2 Optimization of synthesis parameters A) %doping of Tb^{3+} and B) amount of PEG in the reaction medium

Characterization of the as-synthesized PEG-Tb-$CaWO_4$ NCs

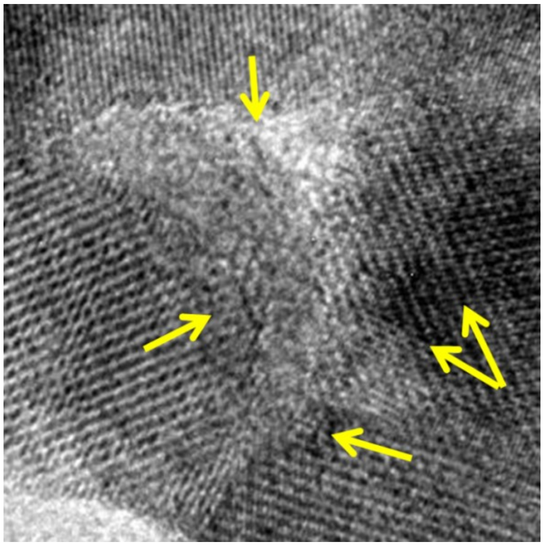

Fig. S3 HR-TEM image showing poly-crystalline nature of the PEG-Tb-$CaWO_4$ NCs.

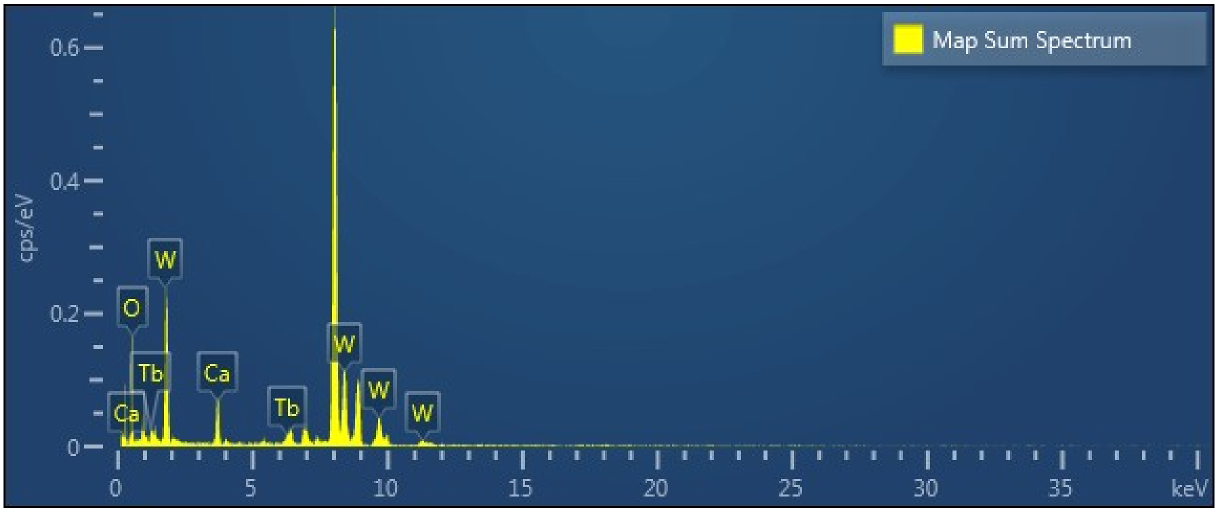

Fig. S4 Energy dispersive X-ray (EDS) spectrum of the PEG-Tb-$CaWO_4$ NCs.

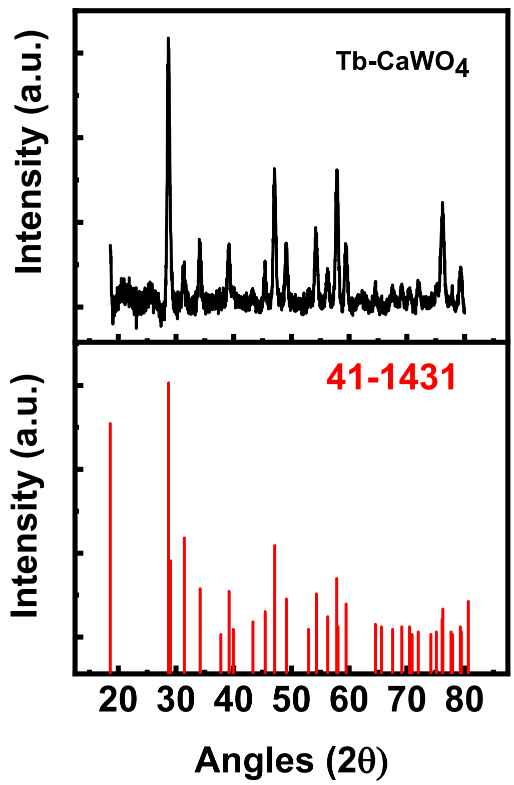

Fig. S5 XRD patterns of the Tb-$CaWO_4$ NCs and the standard diffraction pattern of $CaWO_4$ NCs.

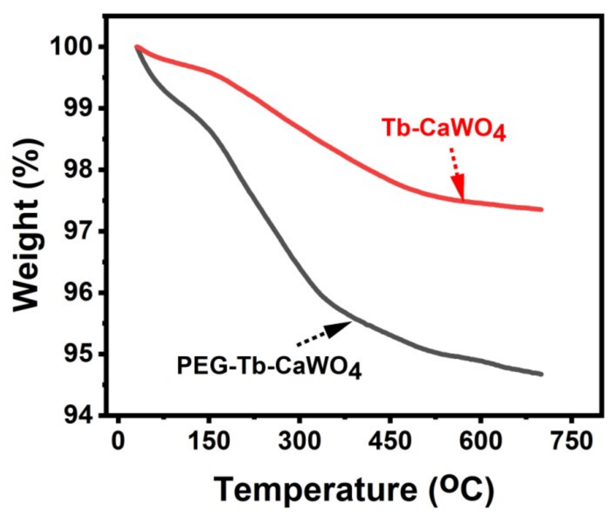

Fig. S6 Thermal gravimetric analysis (TGA) of bare and PEG coated Tb-$CaWO_4$ NCs.

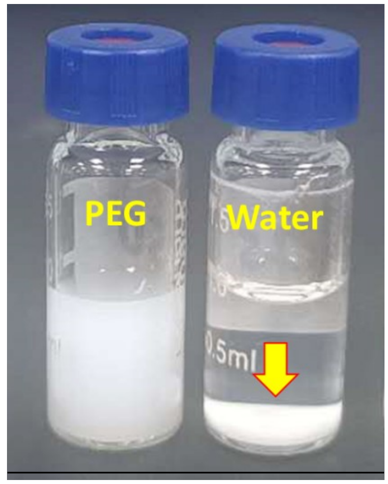

Fig. S7 A) Aqueous dispersion of PEG-coated (left) and uncoated (right) Tb-$CaWO_4$ NCs.

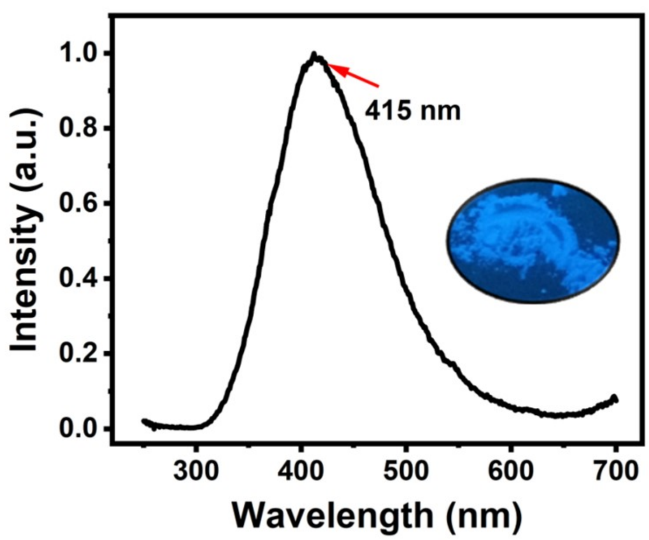

Fig. S8 Fluorescence emission of $CaWO_4$ and Inset: corresponding solid-state luminescence under excitation of 254 nm UV-light.

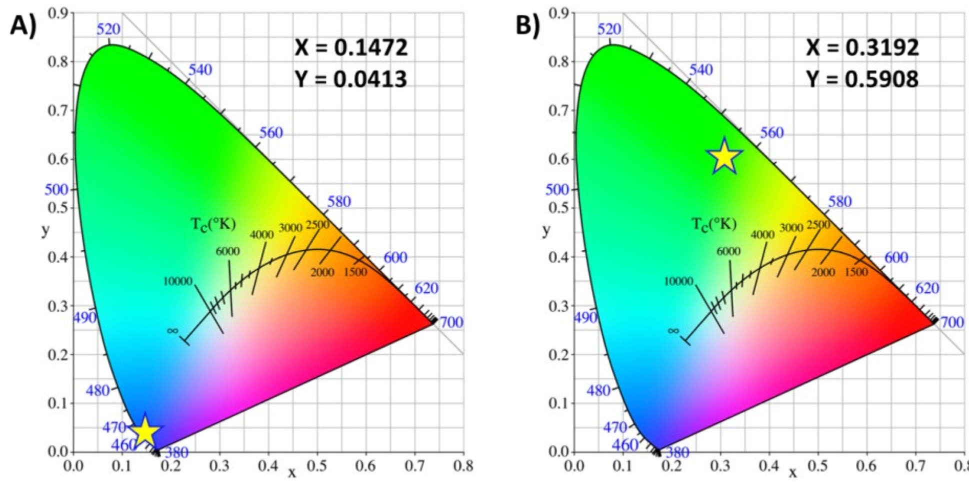

Fig. S9 CIE chromaticity diagram of A) $CaWO_4$ and B) PEG-Tb-$CaWO_4$ NCs. Insets show corresponding fluorescence emission coordinates.

Stability of PEG-**Tb-$CaWO_4$ NCs**

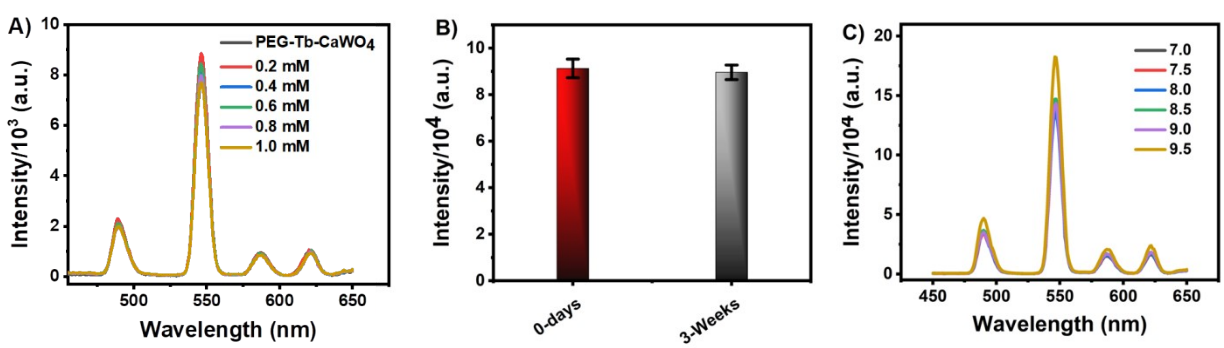

Fig. S10 Stability of the fluorescence intensity of PEG-Tb-$CaWO_4$ NCs against A) various ionic concentrations, B) storage time at 4^{o}C, and C) various pH solutions.

Designing PEG-Tb-$CaWO_4$ NCs based sensor for ALP Detection

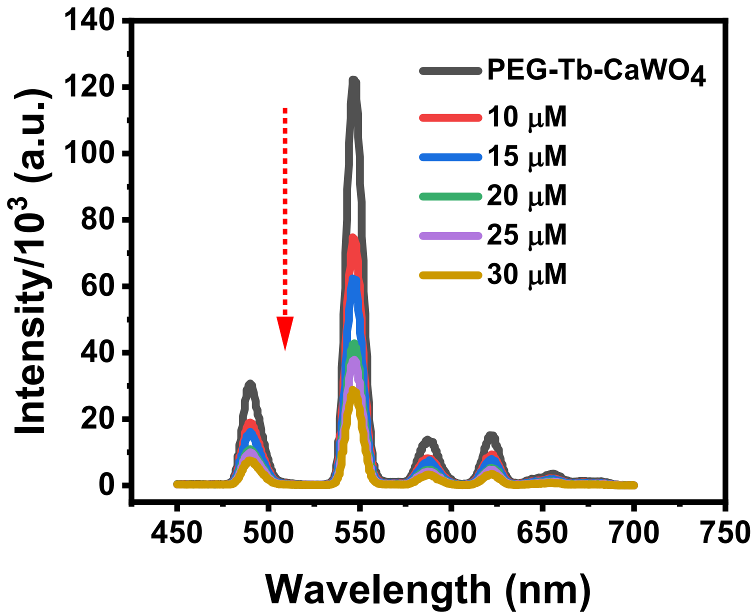

Fig. S11 Fluorescence emission intensity of PEG-Tb-$CaWO_4$ NCs with various concentrations of Ce^{4+} ions.

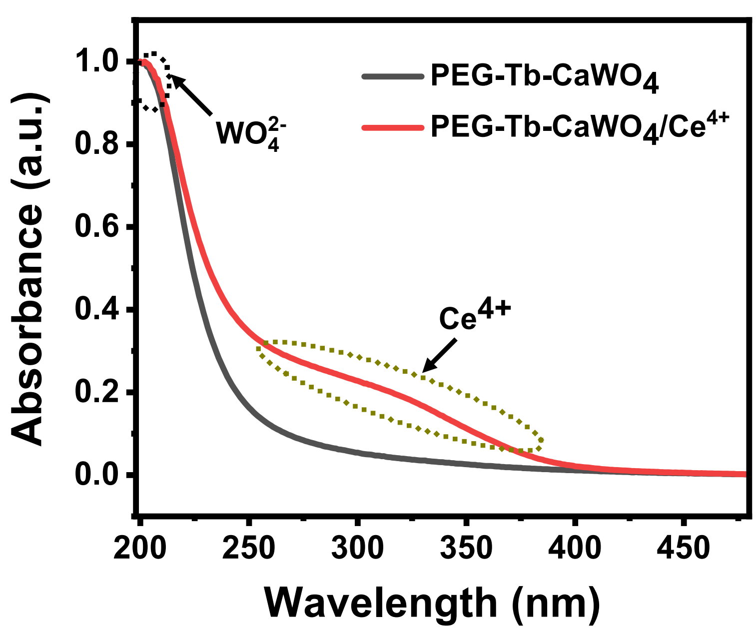

Fig. S12 UV-Visible absorption spectrum of PEG-Tb-$CaWO_4$ NCs with and without the addition of Ce^{4+} ions.

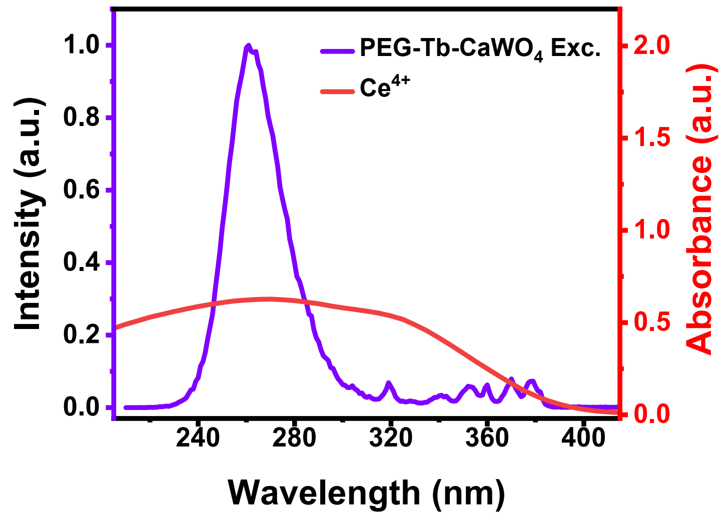

Fig. S13 Fluorescence excitation spectrum of PEG-Tb-$CaWO_4$ NCs and UV-visible absorption spectrum of Ce^{4+} ions.

Optimization of detection conditions

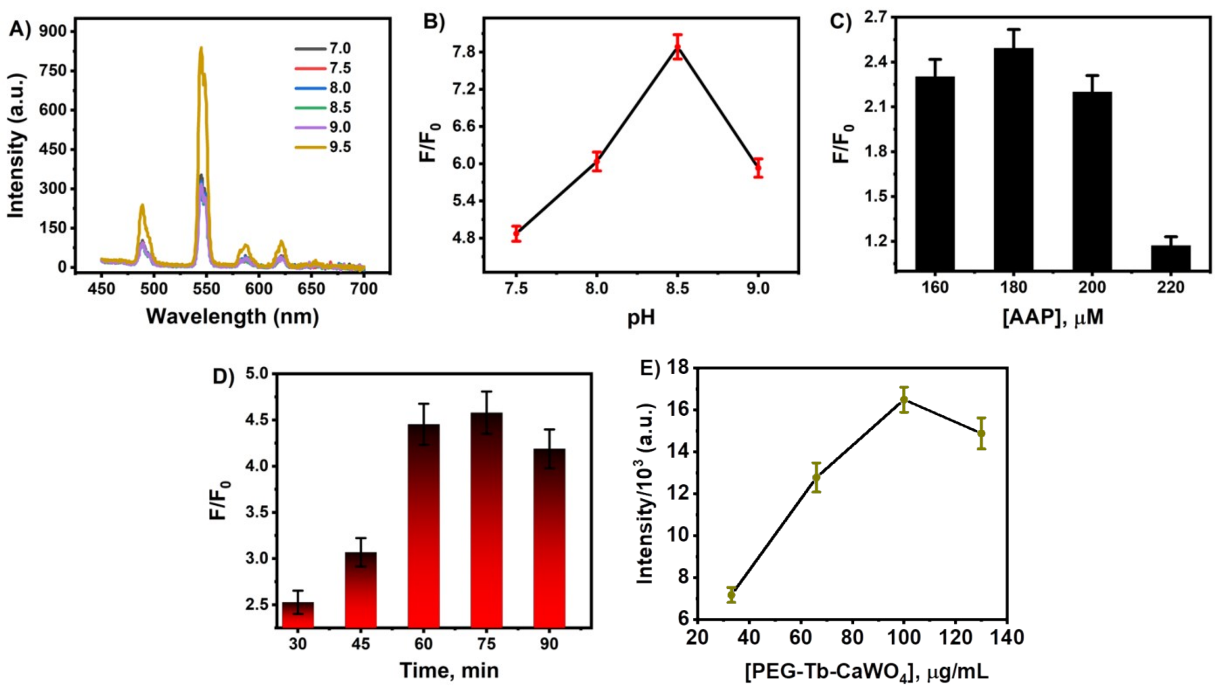

Fig. S14 Optimization of detection conditions A) Effect of pH on fluorescence quenching efficiency of Ce^{4+} ions in the absence of ALP. B) Effect of pH on the fluorescence recovery of the detection system in the presence of ALP. C) Concentration of AAP. D) Enzymatic reaction time. E) Amount of PEG-Tb-$CaWO_4$ NCs.

Optimization of ratio of AA-to-Ce^{4+}

Redox reaction between Ce^{4+} ions and AA. [1]

$$2Ce^{4+} + C_6H_8O_6 \rightarrow 2Ce^{3+} + C_6H_6O_6 + 2H^+ \qquad (S1)$$

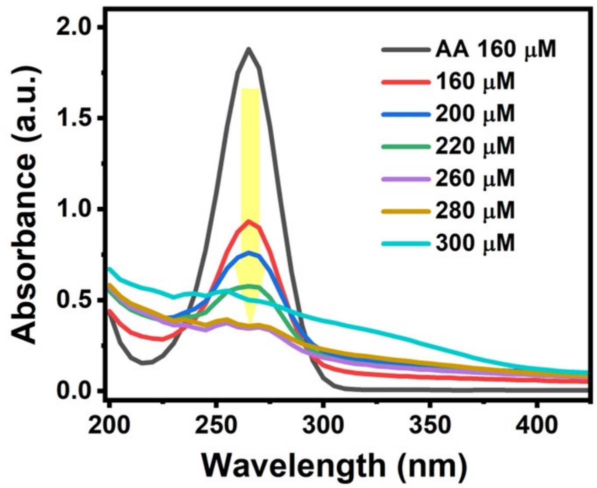

Fig. S15 UV-Vis absorption spectra showing optimization of the ratio (concentrations) of AA-to-Ce^{4+} ions.

Cell viability assay

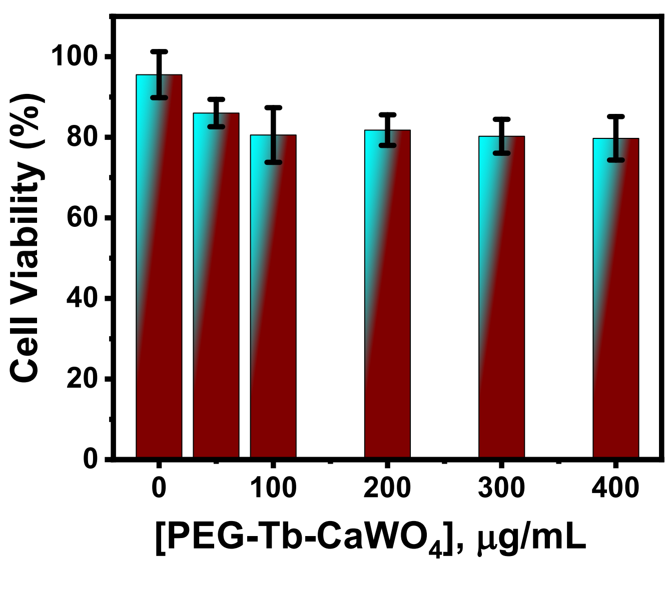

Fig. S16 MTT assay of HeLa cell viability after incubation with PBS (control) and PEG-Tb-$CaWO_4$ NCs at the concentration range of 0–400 μg/mL for 24 h.

Table S1. Comparison of ALP detection method

Method	Sensing Material	LOD (U/L)	Linear range (U/L)	Reference
Colorimetry	Fe/C NS	0.03	0.05 - 6.00	[2]
Colorimetry	Ag NPs	0.24	0.5 - 225	[3]
Electrochemistry	AuNPs/Ag^{+}	0.03	0.1 - 120	[4]
Electrochemistry	Luminol Si NPs	0.8	5 - 50	[5]
Fluorescence	Au/Ag NCs	0.193	0.5 - 10	[6]
Fluorescence	(PAA)-Ca^{2+}(Ce^{3+}) NCs	0.62	5.0 - 200	[7]
Fluorescence	Au NCs-MnO_2 NSs	1.5	5-800	[8]
Fluorescence	CQDs	5.5	18.2–1300	[9]
Fluorescence	E)-8-((4-methylbenzylidene) amino) napthalen-1-amine (L)	50	400-3000	[10]
Fluorescence	Allosteric probe (AP)	12	20-150	[11]
Fluorescence	Pyrococcus furiosus argonaute	2.7	10-1000	[12]
Fluorescence	PEG-**Tb-$CaWO_4$ NCs**	**0.5**	**6 - 40**	**This Work**

Table S2. Determination of ALP in fetal bovine serum samples using the proposed method (n=3)

Sample	Added ALP (U/L)	Detected ALP (U/L)	Recovery (%)	RSD (%)
1	-	-	-	-
2	10	10.77 ± 0.02	107.68	1.61
3	16	13.83 ± 0.03	86.47	1.52
4	20	16.78 ± 0.05	83.89	2.11

References

1. N. K. Sahu, N. Shanta Singh, R. S. Ningthoujam and D. Bahadur, Ce^{3+}-Sensitized GdPO4:Tb^{3+} Nanorods: An Investigation on Energy Transfer, Luminescence Switching, and Quantum Yield, *ACS Photonics*, 2014, **1**, 337-346.
2. X. Chen, J. Chen, H.-Y. Zhang, F.-B. Wang, F.-F. Wang, X.-H. Ji and Z.-K. He, Colorimetric Detection of Alkaline Phosphatase on Microfluidic Paper-based Analysis Devices, *Chinese Journal of Analytical Chemistry*, 2016, **44**, 591-596.
3. S. M. Shaban, B.-S. Moon, D.-G. Pyun and D.-H. Kim, A colorimetric alkaline phosphatase biosensor based on p-aminophenol-mediated growth of silver nanoparticles, *Colloids and Surfaces B: Biointerfaces*, 2021, **205**, 111835.
4. J. Lei, J. Kang, J. Liu and G. Wang, A Novel Electrochemical Sensing Strategy Based on Poly (3,4-ethylenedioxythiophene): Polystyrene Sulfonate, AuNPs, and Ag+ for Highly Sensitive Detection of Alkaline Phosphatase, *Nanomaterials*, 2022, **12**, 3392.
5. W. Qi, Y. Fu, M. Zhao, H. He, X. Tian, L. Hu and Y. Zhang, Electrochemiluminescence resonance energy transfer immunoassay for alkaline phosphatase using p-nitrophenyl phosphate as substrate, *Analytica Chimica Acta*, 2020, **1097**, 71-77.
6. M. Wang, X. Zhou, L. Cheng, M. Wang and X. Su, Lysozyme-Functionalized 5-Methyl-2-thiouracil Gold/Silver Nanoclusters for Luminescence Assay of Alkaline Phosphatase, *ACS Applied Nano Materials*, 2021, **4**, 9265-9273.
7. Y. Fan, Z. Ding, J. Chen, C. Li and Y. Han, Polyacrylic Acid-Ca^{2+}(Ce^{3+}) Nanoclusters as Fluorescent “Off–On–Off” Probes for Quantitative Detection of Pyrophosphate and Alkaline Phosphatase, *ACS Applied Nano Materials*, 2024, **7**, 5678-5688.
8. Y. Xue, C. Bao, H. Liu, F. Ma, M. Yang and X. Li, BSA-Assisted Synthesis of Au Nanoclusters/MnO2 Nanosheets for Fluorescence “Switch-On” Detection of Alkaline Phosphatase, 2025, **15**, 49.
9. Z. Qian, L. Chai, Q. Zhou, Y. Huang, C. Tang, J. Chen and H. Feng, Reversible Fluorescent Nanoswitch Based on Carbon Quantum Dots Nanoassembly for Real-Time Acid Phosphatase Activity Monitoring, *Analytical Chemistry*, 2015, **87**, 7332-7339.
10. S. Kiran, R. Khatik and R. Schirhagl, Smart probe for simultaneous detection of copper ion, pyrophosphate, and alkaline phosphatase in vitro and in clinical samples, *Analytical and Bioanalytical Chemistry*, 2019, **411**, 6475-6485.
11. J. Guo, M. Gao, Y. Song, L. Lin, K. Zhao, T. Tian, D. Liu, Z. Zhu and C. J. Yang, An Allosteric-Probe for Detection of Alkaline Phosphatase Activity and Its Application in Immunoassay, 2018, **6**, 618.
12. Z. Huang, L. Wei, Y. Zhou, Y. Li and Y. Chen, Guide DNA dephosphorylation-modulated Pyrococcus furiosus Argonaute fluorescence biosensor for the detection of alkaline phosphatase and aflatoxins B1, *Biosensors and Bioelectronics*, 2024, **265**, 116692.